PCCP

ROYAL SOCIETY OF CHEMISTRY

PAPER

View Article Online
View Journal | View Issue

Cite this: *Phys. Chem. Chem. Phys.*, 2024, **26**, 8695

Single-crystal growth, structure and thermal transport properties of the metallic antiferromagnet Zintl-phase β-$EuIn_2As_2$†

D. S. Wu,* [ab] S. H. Na,[ab] Y. J. Li,[ab] X. B. Zhou,[ab] W. Wu,[ab] Y. T. Song,[ab] P. Zheng,[ab] Z. Li[abc] and J. L. Luo*[abc]

Received 18th September 2023,
Accepted 31st October 2023

DOI: 10.1039/d3cp04524b

rsc.li/pccp

Zintl-phase materials have attracted significant research interest owing to the interplay of magnetism and strong spin–orbit coupling, providing a prominent material platform for axion electrodynamics. Here, we report the single-crystal growth, structure, magnetic and electrical/thermal transport properties of the antiferromagnet layer Zintl-phase compound β-$EuIn_2As_2$. Importantly, the new layered structure of β-$EuIn_2As_2$, in rhombohedral ($R\bar{3}m$) symmetry, contains triangular layers of Eu^{2+} ions. The in-plane resistivity $\rho(H, T)$ measurements reveal metal behavior with an antiferromagnetic (AFM) transition ($T_N \sim 23.5$ K), which is consistent with the heat capacity $C_p(H, T)$ and magnetic susceptibility $\chi(H, T)$ measurements. Negative MR was observed in the temperature range from 2 K to 20 K with a maximum MR ratio of 0.06. Unique $4f^7$ $J = S = 7/2$ Eu^{2+} spins were supposed magnetically order along the c-axis. The Seebeck coefficient shows a maximum thermopower $|S_{max}|$ of about 40 μV K^{-1}. The kink around 23 K in the Seebeck coefficient originates from the effect of the antiferromagnetic phase on the electron band structure, while the pronounced thermal conductivity peak at around 10 K is attributed to the phonon–phonon Umklapp scattering. The results suggest that the Eu^{2+} spin arrangement plays an important role in the magnetic, electrical, and thermal transport properties in β-$EuIn_2As_2$, which might be helpful for future potential technical applications.

I. Introduction

Since the discovery of Z_2 topological insulators (TI), topology and magnetism have attracted much attention in condensed matter physics and quantum materials science in recent decades.[1–5] Materials with nontrivial band topology of Bloch electrons give birth to many new classifications of quantum matter state, such as Dirac, Weyl, topological crystal insulators, higher-order topological insulators, axion TI and unconventional fermion semimetals.[6–12] Many rare-earth-based magnetic materials also belong to this category and have been reported to host novel electronic states through a complex interplay of magnetism, spin–orbit coupling (SOC), and band topology, such as magnetic Weyl semimetals $Co_3Sn_2S_2$, $MnSb_2Te_4$, and $EuSn_2As_2$.[13,14] The Zintl phase compounds typically consist of separate cations, such as an alkali or alkali-earth metal, with a strongly covalently bonded anionic framework, and are known to exhibit exotic physical properties like colossal magnetoresistance, quantum anomalous Hall effect and spin Hall effect, with applications ranging from thermoelectricity to superconductivity, spintronics and optoelectronics.[15]

Recently, Eu-based Zintl phase materials of the form MX_2Pn_2 (where M represents an alkali-earth metal or europium, X = In or Sn, Zn, Mn, Mg, and Pn = P, As, or Sb) have been predicted to be likely to exhibit topological quantum effects, such as the quantum anomalous Hall effect, Majorana bound states and axion insulator states.[16–19] For example, $EuSn_2As_2$ has been confirmed to be an intrinsic magnetic topological insulator by combining first-principles calculations and angle resolved photoemission spectroscopy measurements.[14] A new monoclinic $EuSn_2As_2$ structure in $C2/m$ symmetry was recently discovered *via* a two-stage reconstruction mechanism under pressure.[17] $EuSn_2P_2$ has been reported to be a type-II nodal-line semimetal when spin–orbit coupling is ignored. Electronic structure calculations reveal that $EuSn_2P_2$ is an antiferromagnetic topological insulator when Hubbard U is included.[18] $EuIn_2As_2$ with lattice constants $a = 4.2107(3)$ Å and $c = 17.9150(2)$ Å and the

[a] *Beijing National Laboratory for Condensed Matter Physics, Institute of Physics, Chinese Academy of Sciences, Beijing 100190, China. E-mail: dswu@iphy.ac.cn, jlluo@iphy.ac.cn*
[b] *School of Physical Sciences, University of Chinese Academy of Sciences, Beijing 100190, China*
[c] *Songshan Lake Materials Laboratory, Dongguan, Guangdong 523808, China*

† Electronic supplementary information (ESI) available. CCDC 2286016. For ESI and crystallographic data in CIF or other electronic format see DOI: https://doi.org/10.1039/d3cp04524b

number of formula units $Z = 3$ in hexagonal $P6_3/mmc$ (no. 194) symmetry was found to exhibit negative colossal magnetoresistance and predicted to exhibit Dirac surface states with energies within the bulk band gap from theoretical calculations.[19,20] Moreover, Angle Resolved Photoemission Spectroscopy experiment showed a linear energy dispersion across the Fermi level with a hole-type Fermi pocket in $EuIn_2As_2$.[21] In another work, an anomalous Hall effect (AHE) originating from a nonvanishing net Berry curvature due to the helical spin structure and a large topological Hall effect (THE) were observed in $EuIn_2As_2$ single-crystal.[22]

For the purposes of discovering new structures, further understanding the magnetic exchange between alkali atoms, and exploring the interplay of magnetism and superconductivity with the band topology in rare earth Zintl phase, our attention is focused on the Eu–In–As system. So far, unique magnetic phenomena have been discovered in the Eu_3InAs_3 system, showing two magnetic orderings characteristic of antiferromagnetic interactions and field-induced metal magnetic transitions.[23,24] On the other hand, the hexagonal $EuIn_2As_2$ has been reported to exhibit low-symmetry helical antiferromagnetic order and field-tunable unpinned Dirac cones, and neutron diffraction, symmetry analysis, and density functional theory study predicted that it is possibly an axion topological insulator.[20,25]

In this work, we successfully grew new Zintl phase $EuIn_2As_2$ single crystals and carried out comprehensive studies on the structure and electrical transport, magnetic susceptibility, heat capacity and thermodynamic properties of the new phase $EuIn_2As_2$ (named β-$EuIn_2As_2$ hereafter). Here we propose that the Eu atoms form a triangular lattice in the ab plane (hexagonal unit cell) with each Eu atom coordinated by six As atoms to form a trigonal prism. The In and As atoms are covalently bonded in a honeycomb arrangement and the In atoms between two adjacent In–As layers face each other with inversion symmetry. In such a lattice geometry, magnetic frustration can arise when the nearest-neighbor exchange interaction between the Eu ions is antiferromagnetic (AFM). We found that the temperature-dependent resistivity exhibits AFM behavior with a peak around 23.5 K, which is similar to the situation for $EuSn_2As_2$.[24] In addition, the magnetic susceptibility results show a possible canted AFM along the *c*-axis with non-collinear magnetic order, but ferromagnetic (FM) in the *ab* plane. A λ-type peak is observed at $T_N = 23.5$ (2) K associated with the AFM ordering from the temperature-dependent specific heat measurements. We propose that the β-$EuIn_2As_2$ exhibits A-type antiferromagnetic order. Furthermore, we also carried out Seeback coefficient and thermal conductivity measurements. We found that the Seeback coefficient is negative at high temperature and its maximum absolute value, $|S_{max}|$, is about 40 μV K^{-1} at 20 K. The thermal conductivity typically first increases to a peak value of 78.8 WK^{-1} m^{-1} and then decreases to a high-temperature value of 19.8 WK^{-1} m^{-1}.

II. Methods

Crystal growth

The single crystalline β-$EuIn_2As_2$ was grown by self-flux method based on previously published procedures.[26] The starting materials, Eu pieces (99.99%, Alfa), In shots (99.999%, Beijing Dream Material Technology Co. Ltd), and As lumps (99.999%, Alfa), were mixed in the mole ratio Eu : In : As 1.05 : 22 : 2 in an Al_2O_3 capsule with a quartz wool filter and sealed with an appropriate amount of Ar atom into a silica tube. Higher reaction temperature was needed to grow β-$EuIn_2As_2$ single-crystal, and the temperature to separate the crystals from the flux is higher compared to the reported phase.[20–22,25] The whole silica tube was then quickly heated up to 1393 K in a furnace and maintained at this temperature for 40 hours. Then the sample was slowly cooled down to 1173 K over more than 200 hours. Then it was cooled down to 973 K at a rate of 1 K h^{-1} where the flux was spun off by a centrifuge. Plate-like black crystals with shiny surface and a typical size of $1 \times 1 \times 0.2$ mm^3 were finally left, shown by the optical microscopy picture in Fig. 1(d). The crystals were stable in air with masses of a few milligrams. We propose that the single-crystal grow process is common and similar to the single-crystal situation of the 1T, 2H, and 3R phases of topological semimetal $MoTe_2$[26] and topological crystal candidate LaSbTe.[28] In addition, the reaction temperature plays an important role in the single-crystal growth process.

Crystal characterization

The crystallographic information framework (CIF) file from a previously published work[27] was used for structural refinement. To confirm the stoichiometry, the chemical compositions of the crystals were confirmed by energy dispersive X-ray spectroscopy (EDS) equipped on a Hitachi S-4800 scanning electron microscope (SEM). Multiple β-$EuIn_2As_2$ crystals ($\sim 1 \times 1 \times 0.5$ mm^3) were tested by single-crystal X-ray diffraction in order to determine the crystal structure of the new material. Single-crystal X-ray diffraction (SCXRD) was performed on a selected small crystal. The crystals were characterized by X-ray diffraction (XRD) at 300 K on a Bruker SMART APEX II diffractometer using Cu $K\alpha_1$ radiation ($\lambda = 1.5406$ Å). The crystal structure data were solved using SHELXT with intrinsic phasing and refined with SHELXL-2017/3 *via* full-matrix least-squares fitting.[29]

Physical property measurements

The magnetization was measured using a Quantum Design magnetic property measurement system (MPMS). The magnetic properties exhibit different behaviors in the *ab* plane and along the *c*-axis. Therefore, an external magnetic field with directions parallel and perpendicular to the *c*-axis of the single-crystal was applied. The temperature dependence of magnetization was measured using a vibrating sample magnetometer (PMMS, Quantum Design Inc.). The measurements were taken under zero-field-cooled and field-cooled conditions in the temperature range 5–300 K and in the applied magnetic fields of 1, 3, and 7 T (1 T = 10^4 Oe). Isothermal magnetization curves were recorded between magnetic fields of ±7 K Oe at temperatures of 5 K and 100 K. A standard four-probe method were used to perform resistivity measurements. Four platinum leads were attached onto a plate-shaped crystal with dimensions of about

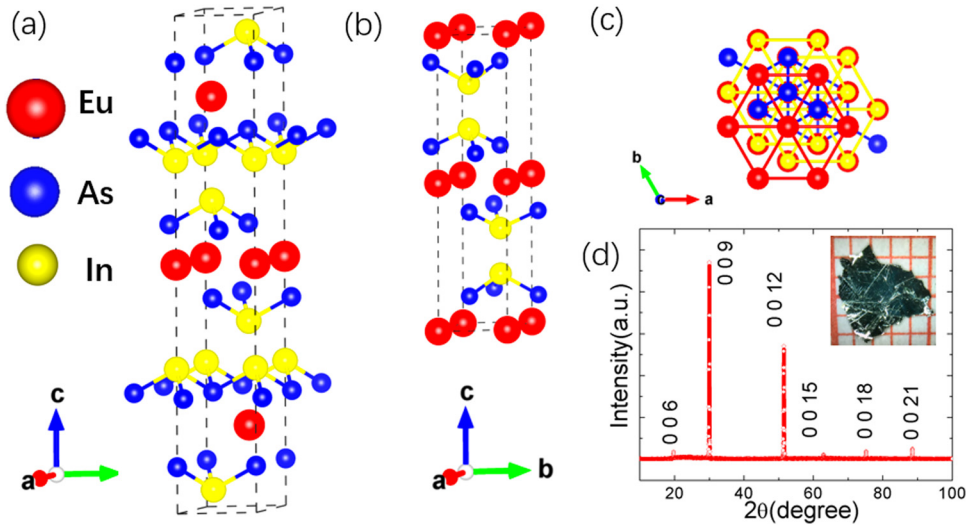

Fig. 1 Crystal structure of β-$EuIn_2As_2$ from different viewpoints, where the red, blue, and yellow represent Eu, As, and In atoms, respectively. (a) Crystal structure of β-$EuIn_2As_2$ with a = 4.2067(3) Å, c = 26.3814(2) Å and Z = 3 in rhombohedral $R\bar{3}m$ (no. 166) symmetry. (b) Crystal structure information of α-$EuIn_2As_2$ with a = 4.2107(3) Å, c = 17.9150(2) Å and Z = 2 in rhombohedral $P6_3/mmc$ (no. 194) symmetry. (c) Top view from (0 0 l) direction for β-$EuIn_2As_2$. (d) Single-crystal X-ray pattern of β-$EuIn_2As_2$ with (0 0 l) direction. The inset is an optical image of the β-$EuIn_2As_2$ single-crystal used in the single-crystal X-ray diffraction measurements.

$1.00 \times 0.51 \times 0.10$ mm^3. A constant current of 1 mA was applied to the sample along the ab plane through the two outer leads. Magnetoresistance was measured under fields of 1, 3, 5 and 7 T. The magnetic field was applied along the c-axis. The temperature dependence of the specific heat (C_p) was measured using a physical properties measurement system (PPMS-9 T, Quantum Design) using the H_C option (relaxation method). The thermal conductivity and Seebeck coefficient of the sample were measured by steady-state method. An E-type thermocouple was used to measure the temperature difference signal, the voltage signal was collected using a Keithley 2182A, and the low-temperature environment is provided by a Quantum Design PPMS system.

III. Results and discussion

Structure and composition of β-$EuIn_2As_2$

We first characterized the structural phase conversion of the layered $EuIn_2As_2$. The single-crystal X-ray diffraction (SCXRD) results for the newly discovered phase of the layered $EuIn_2As_2$ at 293 (2) K are consistent with the previously reported layer structure with rhombohedral symmetry, space group $R\bar{3}m$ (no. 166), with $a = b$ = 4.2067(3) Å, c = 26.3814(2) Å and Z = 3. The detailed crystallographic data and atomic coordinates parameters of the final refinement, which converged to R_1 = 0.036 and ωR_2 = 0.0873, are shown in Tables 1 and 2. We adopted a simple rhombohedral supercell (including 4 Eu, 8 In, and 8 As atoms), as shown in Fig. 1(a), to simulate the interlayer AFM interaction of Eu atoms in the layered β-phase. As a comparison, we also plotted the reported structure of axion topological insulator candidate $EuIn_2As_2$ (termed α-$EuIn_2As_2$ hereafter), with $a = b$ = 4.2107(3) Å, c = 17.9150(2) Å and Z = 2, in hexagonal lattice with the space group $P6_3/mmc$ (no. 194), as shown in Fig. 1(b). In β-$EuIn_2As_2$ (Fig. 1(c)), the Eu atoms form a triangular lattice in the ab plane (hexagonal unit cell) with each Eu atom coordinated by six As atoms forming a trigonal prism. The In and As atoms are covalently bonded in a honeycomb arrangement. The layered features of β-$EuIn_2As_2$, and its in-plane and honeycomb In structure viewed along the c-axis are presented in Fig. 1(c). In such a Kagome lattice geometry, magnetic frustration can arise when the nearest-neighbor exchange interaction between the Eu ions is antiferromagnetic (AFM). The crystalline structure of β-$EuIn_2As_2$ can be viewed as a long chain of $[In_2As_2]^{2-}$ propagating along the c direction, which are separated by individual Eu^{2+} irons in ABC stacking along the c-axis. There is alternate stacking of europium (Eu) cation layers and honeycomb-like InAs anionic

Table 1 Refined crystallographic parameters of β-$EuIn_2As_2$ from single-crystal X-ray structure analysis at 293(2) K

Refined parameter	293(2) K
Empirical formula	β-$EuIn_2As_2$
Formula weight (g mol^{-1})	404.98(5)
Temperature	292 (2 K)
Radiation (wavelength)	Mo Kα (0.7103 Å)
Crystal system	Rhombohedral
Space group	$R\bar{3}m$ (no. 166)
Lattice parameters	a = 4.2102(6) Å α = 90° b = 4.2102(6) Å β = 90° c = 26.3814(2) Å γ = 120°
Cell volume (Å^3)	404.98(5)
Z	3
Density, calculated (g cm^{-3})	6.537
F(0 0 0)	681.00
Index (h, k, l) max	5, 5, 34
2θ range for data collection	5.954° to 56.308°
Absorption correction	Multiscan
T_{min}/T_{max}	0.0278/0.0746
R indexes (all data)	R_1 = 0.0365, ωR_2 = 0.0873
Weighting scheme	$\omega = 1/[\sigma^2(F_o^2) + 0.00739(F_o)^2]$
Refinement software	SHELXL-2017/3

Table 2 Atomic coordinates and equivalent isotropic thermal parameters of β-$EuIn_2As_2$

Atom	Wyckoff	Symmetry	x	y	z	Occup[a]	Ueq[b]
Eu	3a	$\bar{3}m$	1.0000	0	0.5000	1	0.0106
In	6c	$\bar{3}m$	0.667	0.333	0.427	1	0.0127
As	6c	$\bar{3}m$	0.333	0.667	0.376	1	0.0104

[a] Occup: occupancy. [b] Ueq: equivalent isotropic thermal parameter.

bilayers, which are bound by van der Waals (vdW) forces between In cations. Like the Weyl semimetal $MoTe_2$,[26] there are Td, 2H and 3R phases due to the chemical potential being unstable. Layers of In–As–Eu–As–In form a basic unit cell that is repeated three times in β-$EuIn_2As_2$ with a rhombohedral lattice with c/a = 6.271 and the distance between layers is $c/3$ = 8.7938 Å, similar to the 3R phase of $MoTe_2$. Furthermore, layers of Eu–As–In form a basic unit cell that is repeated twice in α-$EuIn_2As_2$ with a hexagonal lattice with c/a = 4.2545 Å and the distance between layers is $c/2$ = 8.9575 Å. Fig. 1(d) shows the single-crystal X-ray diffraction data for β-$EuIn_2As_2$ collected at room temperature in the [0 0 l] direction. The typical size of β-$EuIn_2As_2$ single crystals is 2 × 2 × 0.5 mm, shown by the optical image in the upper inset of Fig. 1(d). The composition was checked by energy dispersive X-ray spectroscopy (EDS) [Fig. S1, ESI†].

Transport properties

We now pay attention to the physical properties of β-$EuIn_2As_2$. Fig. 2(a) shows the temperature-dependent resistivity, $\rho(T)$, of β-$EuIn_2As_2$ from 2 K to 300 K. The resistivity decreases with temperature in the paramagnetic state and the order of magnitude of the resistivity is 5.5 × 10^{-6} Ω cm at T = 300 K, which is in the same order of magnitude as the α phase.[20–22] Around T_N = 23.5 K, the resistance reaches a maximum, followed by a slight drop upon further cooling, exhibiting a metal-like behavior, as shown in Fig. 2(b). This possibly suggests an s–p(d)–f admixture interaction in the magnetic disordered states of this compound like the situation in $EuIn_2P_2$.[30] According to the electrical measurement, one can also see that the AFM order associated with Eu^{2+} moments changes with the application of different magnetic fields. We checked the resistivity under the external magnetic field with the temperature range from 2 K and 50 K. The external magnetic field suppresses the phase transition, and the peak moves to lower temperature with higher fields from 1 T to 7 T, as presented in Fig. 2(c). If we define MR = $[(\rho(H) - \rho(0))/\rho(H)]$, we can plot MR as a function of temperature, as shown in Fig. 2(d). The negative MR can be observed starting from 20 K and increasing to its maximum of −0.06 at around 2 K with 14 T field. After that, the MR drops again with decreasing temperature. The MR magnitude of this compound is much smaller than those of most colossal magnetoresistance (CMR) Zintl compounds with 14–1–11 structure type, like $Eu_{13}CaMnSb_{11}$ (80% at 6 T)[31] and $Eu_{14}MnAs_{11}$ (203% at 5 T).[32] It was proposed that the CMR property in 14–1–11 compounds comes from the s–d interactions based on the RKKY type exchange,[33] while in doped perovskites, the spin alignment of Mn 4d electrons enhanced by the magnetic field favors the electron hopping between Mn and is considered the source of CMR (double exchange).[33] The Zintl phase compound

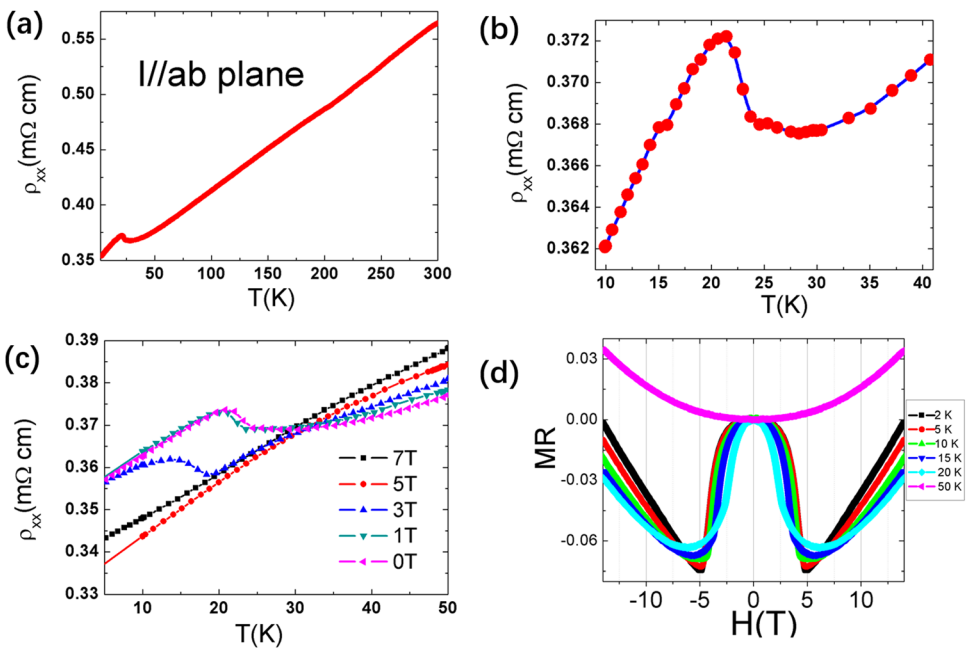

Fig. 2 The charge transport properties of β-$EuIn_2As_2$. (a) The temperature dependence of the (001) plane resistivity ρ_{xx} between 2 K and 300 K in the absence of an applied magnetic field. (b) The expanded plot shows an AFM transition of about 23.5 K. (c) Field dependence of the resistivity ρ_{xx} at various fields. The main panel zooms in on the T range of the main AFM transition, with measurements made in $H//ab$, $H_{\perp}$I of 0 T (black, top curve), 1 T (green), 3T (blue), 5 T (red), and 7 T (black). Note the negative magnetoresistance in the T range below 30 K and the crossover to positive magnetoresistance above. (d) The field-dependent magnetoresistance (MR) for various temperatures (2 K, 5 K, 10 K, 15 K, 20 K and 50 K) on sweeping the applied field from 9 T to −9 T.

β-$EuIn_2As_2$ is different from either of the above two types of compounds by not containing a transition metal. The large MR in this compound should be related to the interaction between the f moments from the Eu^{2+} and the conduction electrons. The external magnetic field boosts the ferromagnetic alignment of the f moments and thus decreases the scattering of the conduction electrons by disordered local moments. Another reasonable interpretation is from the topology band structure point of view. Increasing the external magnetic field can enhance the magnetic order. As a result, the conduction band goes through a strong splitting and crosses the valence band, possibly forming a nontrivial topological band. If the band crossovers are quite near the Fermion level, this has a strong effect on the electronic transport properties. The resistance behavior of β-$EuIn_2As_2$ is similar to the resistance behavior of topological material candidate LaSbTe, whereby different phase structures with the same stoichiometry exhibit different topological properties. For example, tetragonal-LaSbTe was predicted to be a weak topological insulator[34] and this was confirmed by ARPES experiments,[35] while orthorhombic-LaSbTe(o-LaSbTe) was predicted to be topological crystal insulator,[34] and both the t and o phase show metallic resistivity behavior.

Susceptibility

Magnetization measurements offer details on the type of magnetic order in the β-$EuIn_2As_2$ and enable determination of the magnetic diagram. Temperature-dependent magnetic susceptibility, measured with an applied field perpendicular and parallel to the *c*-axis, is shown in Fig. 3(a). A kink, shown at T_N = 23.5 K under H = 10 k Oe in the $\chi(T)$ curve, indicates a clear antiferromagnetic phase transition. The AFM transition is also confirmed by the data from the $C_p(T)$ curves measured at zero field, showing a λ-type anomaly around 23.5 K [see Fig. 4(c)]. There is a small tail in the $\chi - (T)$ curve near 2 K, which might be contributed by magnetic impurity effects. The inset in Fig. 3(a) displays the χ–(T) curves for β-$EuIn_2As_2$ measured under a magnetic field of 10 k Oe with $H//ab$ plane and $H//c$-axis, respectively. Fitting the 50 K to 300 K data with the Curie–Weiss law, $\chi = C/(T - \theta_W)$,[27] where C and θ_W are the Curie constant and the Weiss temperature, respectively, and values of C_{ab} = 5.01 emu K mol^{-1} and θ_{ab} = 21.53 K were obtained for the $H//ab$ plane and C_c = 6.83 emu K mol^{-1} and θ_C = 8.47 K for the $H//c$-axis. According to the C values, effective moments μ_{eff} of 6.33 μ_B/Eu^{2+} and 7.39 μ_B/Eu^{2+} were obtained for $H//ab$ and $H//c$, respectively, which are close to the theoretical value of 7.94 μ_B for Eu^{2+} spins with S = 7/2 and g = 2. The positive values of θ_{ab} and θ_C indicate dominant ferromagnetic (FM) interactions between the Eu spins. In combination with the observed antiferromagnetic order, this implies a mixture of magnetic exchange interactions. The effective moments, μ_{eff}, are comparable with the values reported for other Eu-based compounds $EuIn_2P_2$, Eu_3InAs_3, and $EuSn_2As_2$.[16,20–27,30] Another noticeable feature in the susceptibility data is the anisotropy in the $\mu_0H//ab$ plane and $\mu_0H//c$-axis in Fig. 3(a). The anisotropy is larger below the T_N in comparison to above the T_N; this anisotropy is not due to demagnetization, which has been subtracted from the data, and instead implies spin alignment in the *ab* plane below T_N. These features are in agreement with the observations on other related Eu compounds.[20–27,30]

To further study the field-induced magnetic states in β-$EuIn_2As_2$, isothermal magnetization curves, M(H), were measured at 5 K with the $H//ab$ plane and $H//c$-axis. The magnetization *versus* field measurements for both directions at 5 K are shown in Fig. 3(b). In both crystal directions, we did not obtain the absolute saturations of the magnetization. This unsaturation rules out the possibility of mixed valency of Eu^{2+}/Eu^{3+}, which needs further explanation. No clear hysteresis and highly linear $M(H)$ behavior in $\chi(H)$ can be seen at the low-field area in the $\mu_0H//ab$ plane and $\mu_0H//c$-axis directions, similar to many other Eu-based materials.[20–27] However, there are obvious differences in the $M(H)$ data in the $H//ab$ plane and $H//c$-axis directions. The magnetic curve $M(H)$ starts to saturate at around 4.23 T when the magnetic field is parallel to the

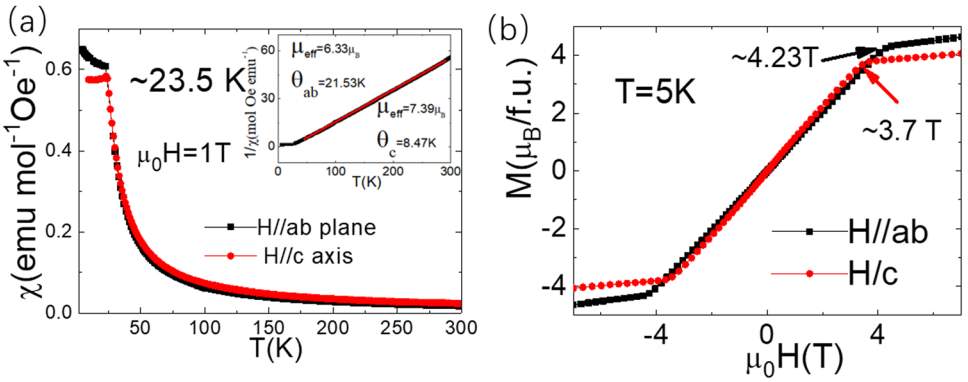

Fig. 3 The field-dependent, direction-dependent, and temperature-dependent magnetic properties of β-$EuIn_2As_2$. (a) Magnetic susceptibility as a function of temperature measured in an external field of μ_0H = 1 Tesla, both perpendicular (black) and parallel (red) to the *c*-axis. The inset shows the temperature-dependent inverse susceptibility, measured for different sample orientations. The red line is the Curie–Weiss fit to the high-temperature data. (b) The field-dependent magnetization for β-$EuIn_2As_2$ measured at 5 K where red balls and black squares represent magnetic field parallel and perpendicular to the *c*-axis, respectively.

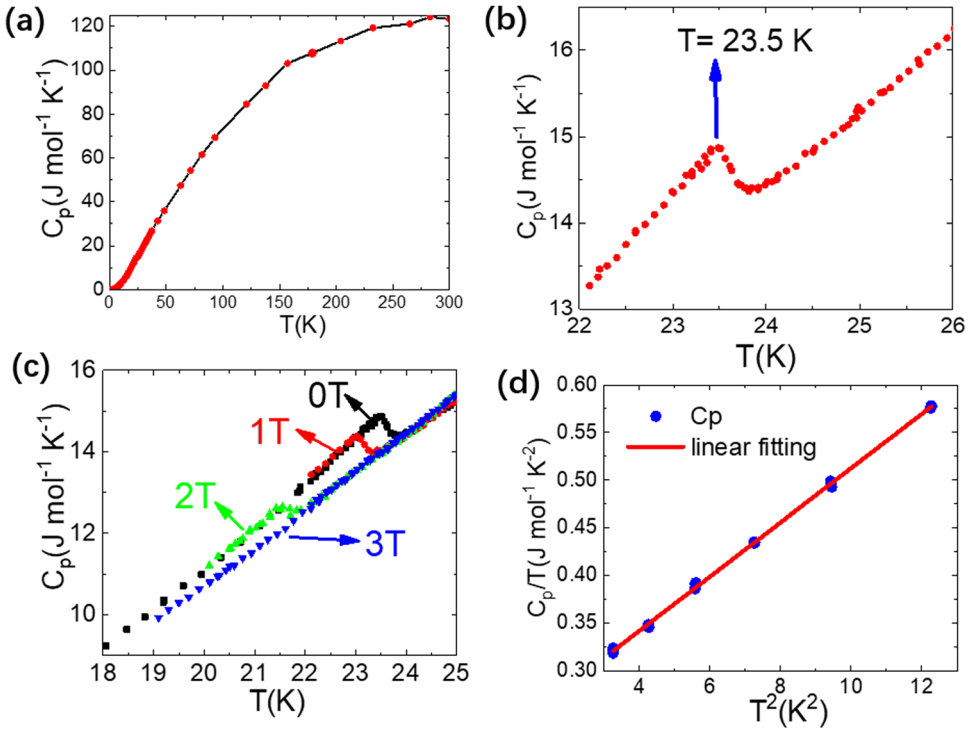

Fig. 4 Heat capacity C_p of β-$EuIn_2As_2$ with and without magnetic fields. (a) Temperature dependence of zero-field heat capacity C_p for β-$EuIn_2As_2$ single crystal; the jump in the data at ≈290 K is an experimental artifact. (b) Expanded plot of the data between 20 K and 30 K shows the peak at about 23.5 K. (c) Plot of C_p (T) of β-$EuIn_2As_2$ crystal measured for different applied magnetic fields with C_p (T) showing the suppression of the AFM ordering temperature T_N with increasing H. (d) Fitting curve of the low-temperature specific heat in the form C_p/T *vs.* T^2 below 10 K, with formula $C_p/T = \beta T^2 + \gamma$.

ab plane, while saturation happens at around 3.70 T in the $\mu_0 H//c$-axis direction. The signs of saturation appear at different magnetic fields, which means that there is a difference in the magnetic stiffness in the $H//ab$ plane and $H//c$-axis. These anisotropic features are consistent with the susceptibility results in Fig. 3(a). This behavior implies higher anisotropy in-plane than out of plane. The positive θ_W is usually attributed to ferromagnetic interactions. From $M(T)$, we can observe that the overall magnetic order is most definitely antiferromagnetic (the sharp peak is attributed to T_N). However, if we look at individual Eu layers, it is apparent that the Eu atoms within a plane are ferromagnetically coupled to one another, whereas each layer is antiferromagnetically coupled to adjacent layers. Another feature is that the Eu spins in the α phase do not undergo any apparent phase transitions. A reasonable way to explain these magnetic properties is an AFM transition with FM correlation. Below the magnetic transition temperature, magnetic moments align in the same direction within the *ab* plane. Because the Eu–Eu distance is relatively large, direct magnetic exchange should be weak. Indirect Eu–Eu interaction through phosphorus is possible between two Eu^{2+} ions in the same layer but is not likely between Eu^{2+} atoms in different layers. Indirect Eu–Eu interaction through phosphorus is possible between two Eu^{2+} in the same layer but is not likely between Eu^{2+} in different layers. The order cannot be G type (all antiferromagnetic within and between Eu layers), since in that case a proper phase transition should be observed with an applied field. The triangular lattice within each layer makes C-type order (ferromagnetic between layers, antiferromagnetic within layers) unlikely as there is no evidence of a structural phase transition. Further, with C-type order one would expect a field-driven magnetic transition along one of the two directions, while none are observed. We are thus left with A-type order (ferromagnetic layers stacked antiferromagnetically) as the prime candidate for the magnetic order. Such an order can continuously rotate to a field-polarized state independent of the applied field direction. It is also similar to the known magnetic order in isostructural Eu-based Zintl compounds.[21–23,27]

Specific heat

The temperature-dependent specific heat ($C_p(T)$) of β-$EuIn_2As_2$ at different applied magnetics fields with $H//c$ is plotted in Fig. 4. A λ-type peak is observed at T_N = 23.5 K associated with the AFM ordering. The $C_p(T)$ value of ≈123 J mol^{-1} K^{-1} at T = 300 K is close to the classical high-T Dulong–Petit limit C_V = $3nR$ = 124.71 J mol^{-1} K^{-1} associated with lattice vibrations for this compound, where n = 5 is the number of atoms per formula unit and R is the molar-gas constant. The bump in the plot of C_p *versus* (T) at around T = 290 K is an instrumental artifact arising from melting of the Apiezon N grease used for making thermal contact between the crystal and the sample platform of the heat capacity puck. The data in Fig. 4(c) show that antiferromagnetic order with Néel temperature T_N = 23.5 K shifts to lower T with increasing H, as expected. It is reasonable to describe the specific heat of the samples as the sum of electronic, lattice, and magnetic contributions. At low

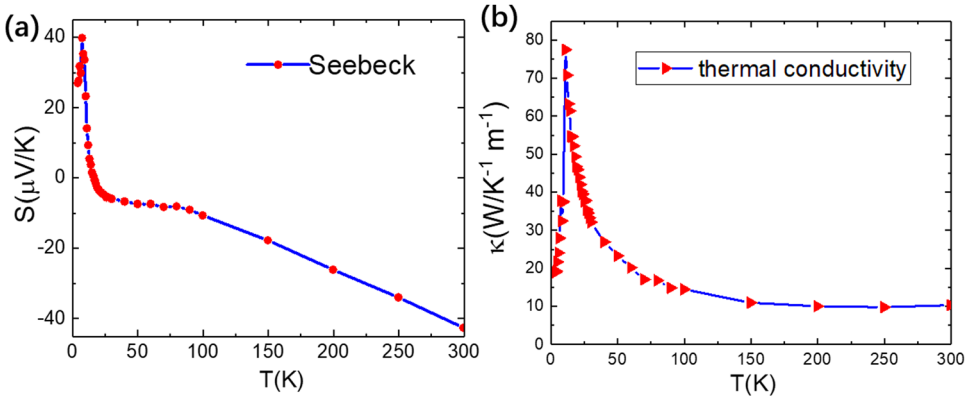

Fig. 5 (a) Temperature dependence of the thermopower $S(T)$ and thermal conductivity $k(T)$ of β-$EuIn_2As_2$ single crystals from 2 K to 300 K. (b) Temperature dependence of the d thermal conductivity $k(T)$ of β-$EuIn_2As_2$ single crystals from 2 K to 300 K.

temperatures, we fit the data with formula $C_p/T = \beta T^2 + \gamma$. The low-temperature specific heat in the form C_p/T *vs.* T^2 below 10 K is shown by Fig. 4(d). The linear trend of the plots at very low temperatures indicates that the Debye approximation may characterize the temperature dependence of C_p. The least-squares analysis of the linear part using the formula, where β and γ are the lattice and electronic contributions to the C_p, respectively, yielded $\gamma \approx 0.27$ mJ mol^{-1} K^{-2}. The non-zero γ value shows a really small considerable density of states (DOS) at E_F, indicating a metallic behavior of β-$EuIn_2As_2$. These resistivity, susceptibility and specific heat measurements suggest that a possible A-type AFM phase transition happened at $T_N = 23.5$ K. We suppose such a behavior may be understood by the electronic structure in β-$EuIn_2As_2$. The band structure calculations with spin–orbit coupling for β-$EuIn_2As_2$ are needed to better understand the electronic structures and physical properties.

Thermoelectric property

The temperature dependence of the Seebeck coefficient for β-$EuIn_2As_2$ is shown in Fig. 5(a). The temperature-dependent Seebeck coefficient for α measured between 2 K and 300 K is shown in Fig. 5(a). Negative Seebeck coefficient values are observed for the high-temperature range measured, indicating that the charge carriers are dominantly electrons. The β-$EuIn_2As_2$ displays large Seebeck coefficient between −40 and 40 μV K^{-1} from room temperature to 2 K. The Seebeck coefficient increases with the decrease of temperature in the range of 90–300 K and decreases slowly in the range of 16–90 K. The Seebeck coefficient increases rapidly with decreasing temperature after changing sign at 16 K until it reaches a peak at 7 K and then decreases. We tried to measure the Hall resistivity of β-$EuIn_2As_2$ samples from room temperature to low temperatures and found that the Hall sign was too small to measure, indicating that the as-grown β-$EuIn_2As_2$ single crystals possibly have a large carrier concentration. The temperature-dependent thermal conductivity $k(T)$ was measured in the temperature range of 2–300 K, as shown in Fig. 5(b). The thermal conductivity shown in Fig. 5(b) could be regarded as mainly dominated by the lattice contribution. With increasing temperature, the thermal conductivity undergoes a typical first increase to a peak value of 78.8 WK^{-1} m^{-1} and then decreases to an asymptotic high-temperature value of 19.8 WK^{-1} m^{-1}. The decreasing of thermal conductivity in the high-temperature range is mainly due to the phonon–phonon Umklapp scattering.

VI. Conclusion

In conclusion, we reported a new structure of Zintl phase β-$EuIn_2As_2$ by self-flux method. The β-$EuIn_2As_2$ compound crystallized into the structure of rhombohedral $R\bar{3}m$ (no. 166) symmetry. We studied the electron transport, heat capacity, magnetic, thermal transport properties of the β-$EuIn_2As_2$, and discovered an antiferromagnetic order with $T_N = 23.5$ K. *Via* magnetic susceptibility measurements, the anisotropy of the $\mu_0 H//ab$ and $\mu_0 H//c$ directions of β-$EuIn_2As_2$ single crystals were characterized. Significant anisotropy develops below T_N. The magnetic ordering is proposed to be antiferromagnetic along the unit cell c-axis and ferromagnetic correlation perpendicular to the c-axis. A kink around T_N was found in the temperature-dependent resistivity of β-$EuIn_2As_2$ that is gradually suppressed with increasing H. Negative MR was observed in the temperature range from 2 K to 20 K with a maximum MR ratio of 0.06; the negative MR might origin from the nontrivial band topology or the magnetic exchange interaction. A λ anomaly was observed in the heat capacity at $T_N = 23.5$ K, which is suppressed with applying magnetic field. Measurements of Seebeck coefficients showed that β-$EuIn_2As_2$ has small negative Seebeck coefficients similar to those reported in ref. 25 and 36, which will be helpful for future device applications. Further studies are needed to understand the magnetic ground state, such as neutron diffraction to determine the magnetic structures under varied magnetic fields.

Author contributions

D. S. Wu and J. L. Luo supervised the project. D. S. Wu and S. H. Na grew the single crystals. D. S. Wu, S. H. Na and Y. J. Li carried out the resistivity and heat capacity measurement with

help from Ping Z. D. S. Wu, W. Wu and X. B. Zhou did the Seeback coefficient and thermal conductivity measurements. D. S. Wu, Ping Z., Z. Li and J. L. Luo discussed the data. D. S. Wu wrote the paper with contributions from all the authors.

Conflicts of interest

The authors declare no competing financial interest.

Acknowledgements

We thank Dr Y. J. Xu, Dr J. H. Zhang, Dr Y. T. Qian. Dr J. C. Gao, Prof. G. T. Liu, and Prof. H. M. Weng for physical properties discussions. We are grateful to S. L. Li (Institute of Physics) for his help and discussions regarding the single-crystal X-ray diffraction experiments. This work was supported by the National Key Research and Development Program of China (grant no. 2017YFA0302901), the National Science Foundation of China (grants no. 12134018, 11921004, 11634015), the Strategic Priority Research Program and Key Research Program of Frontier Sciences of the Chinese Academy of Sciences (grant no. XDB33010100), the Postdoctoral Science Foundation of China (grant no. 2021M693370) and the Synergetic Extreme Condition User Facility (SECUF).

References

1 M. Z. Hasan and C. L. Kane, Colloquium: Topological insulators, *Rev. Mod. Phys.*, 2010, **82**, 3045.
2 X. L. Qi and S. C. Zhang, Topological insulators and superconductors, *Rev. Mod. Phys.*, 2011, **83**, 1057.
3 M. G. Vergniory, L. Elcoro, C. Felser, N. Regnault, B. A. Bernevig and Z. Wang, A complete catalogue of high-quality topological materials, *Nature*, 2019, **566**, 480.
4 B. Bradlyn, J. Cano, Z. Wang, M. G. Vergniory, C. Felser, R. J. Cava and B. A. Bernevig, Beyond Dirac and Weyl fermions: Unconventional quasiparticles in conventional crystals, *Science*, 2016, **353**, aaf5037.
5 A. M. Mills, R. Lam, M. J. Ferguson, L. Deakin and A. Mar, *Coord. Chem. Rev.*, 2002, **233–234**, 207–222.
6 J. Shuai, J. M. Song, Q. Zhang, G. Chen and Z. Ren, Recent progress and future challenges on thermoelectric Zintl materials, *Mater. Today, Phys.*, 2017, **1**, 74.
7 B. Xie, H. X. Wang, X. Zhang, P. Zhan, J. H. Jiang, M. Lu and Y. Chen, Higher-order band topology, *Nat. Rev. Phys.*, 2021, **3**(7), 520–532.
8 B. A. Bernevig, F. Claudia and H. Beidenkopf, Progress and prospects in magnetic topological materials, *Nature*, 2022, **603**, 41–51.
9 T. Shang, J. Zhao, L. H. Hu, J. Ma, D. J. Gawryluk, X. Zhu and T. Shiroka, Unconventional superconductivity in topological Kramers nodal-line semimetals, *Sci. Adv.*, 2022, **8**(43), eabq6589.
10 A. B. Sarkar, S. Mardanya, S. M. Huang, B. Ghosh, C. Y. Huang, H. Lin and B. Singh, magnetically tunable Dirac and Weyl fermions in the Zintl materials family, *Phys. Rev. Mater.*, 2022, **6**(4), 044204.
11 Z. Hasan, S. Y. Xu and M. Neupane, Topological insulators, topological Dirac semimetals, topological crystalline insulators, and topological Kondo insulators, *Topological insulators: Fundamentals and perspectives*, 2015, 55–100.
12 B. Bradlyn, J. Cano, Z. Wang, M. G. Vergniory, C. Felser and R. J. Cava, Beyond Dirac and Weyl fermions: Unconventional quasiparticles in conventional crystals, *Science*, 2016, **353**(6299), aaf5037.
13 N. Morali, R. Batabyal, P. K. Nag, E. Liu, Q. Xu, Y. Sun and H. Beidenkopf, Fermi-arc diversity on surface terminations of the magnetic Weyl semimetal $Co_3Sn_2S_2$, *Science*, 2019, **365**(6459), 1286–1291.
14 D.-Q. Zhang, M.-J. Shi, T.-S. Zhu, D.-Y. Xing, H.-J. Zhang and J. Wang, Topological Axion States in Magnetic Insulator $MnBi_2Te_4$ with the Quantized Magnetoelectric Effect, *Phys. Rev. Lett.*, 2019, **122**, 206401.
15 H. Weng, R. Yu, X. Hu, X. Dai and Z. Fang, Quantum anomalous Hall effect and related topological electronic states, *Adv. Phys.*, 2015, **64**(3), 227–282.
16 H. Li, S. Y. Gao, S. F. Duan, Y. F. Xu, K. J. Zhu, S. J. Tian and H. Ding, Dirac surface states in intrinsic magnetic topological insulators $EuSn_2As_2$ and $MnBi_{2n}Te_{3n+1}$, *Phys. Rev. X*, 2019, **9**(4), 041039.
17 L. Zhao, C. Yi and C. T. Wang, Monoclinic $EuSn_2As_2$: A Novel High-Pressure Network Structure, *Phys. Rev. Lett.*, 2021, **126**(15), 155701.
18 X. Gu, I. Pletikosic and H. Cao, A new magnetic topological quantum material candidate by design, *ACS Cent. Sci.*, 2019, **5**(5), 900–910.
19 Y. Xu, Z. Song, Z. Wang, H. Weng and X. Dai, Higher-order topology of the axion insulator $EuIn_2$ As_2, *Phys. Rev. Lett.*, 2019, **122**(25), 256402.
20 A. M. Goforth, P. Klavins, J. C. Fettinger and S. M. Kauzlarich, Magnetic Properties and Negative Colossal Magnetoresistance of the Rare Earth Zintl phase $EuIn_2As_2$, *Inorg. Chem.*, 2008, **47**(23), 11048–11056.
21 Y. Zhang, K. Deng, X. Zhang, M. Wang, Y. Wang, C. Liu, J. W. Mei, S. Kumar, E. F. Schwier, K. Shimada, C. Y. Chen and B. Shen, In-plane antiferromagnetic moments and magnetic polaron in the axion topological insulator candidate $EuIn_2As_2$, *Phys. Rev. B*, 2020, **101**(20), 205126.
22 J. Yan, Z. Z. Jiang, R. C. Xiao, W. J. Lu, W. H. Song, X. B. Zhu, X. Luo, Y. P. Sun and M. Yamashita, Field-induced topological Hall effect in antiferromagnetic axion insulator candidate $EuIn_2As_2$, *Phys. Rev. Res.*, 2022, **4**, 013163.
23 K. Jia, C. X. Wang and X. Dong, Emergence of 1/3 magnetization plateau and successive magnetic transitions in Zintl phase Eu_3InAs_3, *Phys. Rev. Res.*, 2021, **3**(4), 043178.
24 K. Rajput, S. Baranets and S. Bobe, Observation of an unexpected n-type semiconducting behavior in the new ternary Zintl phase Eu_3InAs_3, *Chem. Mater.*, 2020, **32**(22), 9616–9626.
25 S. X. Riberolles, M. Trevisan and V. B. Kuthanazhi, Magnetic crystalline-symmetry-protected axion electrodynamics and field-tunable unpinned Dirac cones in $EuIn_2As_2$, *Nat. Commun.*, 2021, **12**(1), 1–7.

26 H. C. Chen, Z. F. Lou and Y. X. Zhou, Negative magnetoresistance in antiferromagnetic topological insulator $EuSn_2As_2$, *Chin. Phys. Lett.*, 2020, **37**(4), 047201.
27 E. J. Cheng, J. M. Ni, F. Q. Meng, T. P. Ying, B. L. Pan, Y. Y. Huang and S. Y. Li, Nodeless superconductivity in the SnAs-based van der Waals-type superconductor $NaSn_2A_{s2}$, *Europhys. Lett.*, 2018, **123**(4), 47004.
28 M. Q. Arguilla, J. Katoch and K. Krymowski, $NaSn_2As_2$: an exfoliatable layered van der Waals Zintl phase, *ACS Nano*, 2016, **10**(10), 9500–9508.
29 **https://shelx.uni-goettingen.de**.
30 J. Jiang and S. M. Kauzlarich, Colossal magnetoresistance in a rare earth zintl compound with a new structure type: $EuIn_2P_2$, *Chem. Mater.*, 2006, **18**(2), 435–441.
31 A. C. Payne, M. M. Olmstead, S. M. Kauzlarich and D. J. Webb, Structure, Magnetism, and Magnetoresistance of the Compounds $Eu_{14}MnAs_{11}$ and $Eu_{14}MnP_{11}$, *Chem. Mater.*, 2001, **13**(4), 1398–1406.
32 M. M. Kim, P. Olmstead, D. J. Klavins and S. M. Webb, Kauzlarich, Structure, Magnetism, and Colossal Magnetoresistance (CMR) of the Ternary Transition Metal Solid Solution $Ca_{14-x}Eu_xMnSb_{11}$ ($0 < x < 14$), *Chem. Mater.*, 2002, **14**(8), 3382–3390.
33 C. Zener, Interaction between the -Shells in the Transition Metals. II. Ferromagnetic Compounds of Manganese with Perovskite Structure, *Phys. Rev.*, 1951, **82**, 403–405.
34 Y. T. Qian, Z. T. Zhang, Z. Tan, J. C. Gao, Z. J. Wang, Z. Fang, F. Chen and H. M. Weng, *Sci. China: Phys., Mech. Astron.*, 2020, **63**, 107011.
35 Y. Wang, Y. Qian, M. Yang, H. Chen, C. Li, Z. Tan, Y. Cai, W. Zhao, S. Gao, Y. Feng, S. Kumar, E. F. Schwier, L. Zhao, H. Weng, Y. Shi, G. Wang, Y. Song, Y. Huang, K. Shimada, Z. Xu, X. J. Zhou and G. Liu, Spectroscopic evidence for the realization of a genuine topological nodal-line semimetal in LaSbTe, *Phys. Rev. B*, 2021, **103**, 125131.
36 K. Bernot, J. Luzon and R. Sessoli, The canted antiferromagnetic approach to single-chain magnets, *J. Am. Chem. Soc.*, 2008, **130**(5), 1619–1627.